Examining the dynamics of chromosomal passenger complex (CPC)-dependent phosphorylation during cell division

Lei Tan and Tarun M. Kapoor[1]

Laboratory of Chemistry and Cell Biology, The Rockefeller University, New York, NY 10065

Edited by J. Richard McIntosh, University of Colorado, Boulder, CO, and approved August 31, 2011 (received for review April 27, 2011)

The dynamic cellular reorganization needed for successful mitosis requires regulatory cues that vary across microns. The chromosomal passenger complex (CPC) is a conserved regulator involved in key mitotic events such as chromosome–microtubule attachment and spindle midzone formation. Recently, spatial phosphorylation gradients have been reported for CPC substrates, raising the possibility that CPC-dependent signaling establishes order on the micron-length scale in dividing cells. However, this hypothesis has not been tested, largely because of incomplete characterization of the CPC-dependent phosphorylation dynamics. Without these data it is difficult to evaluate perturbations of CPC signaling and select one that alters the spatial organization of substrate phosphorylation at a particular stage of mitosis, without changing overall phosphorylation levels. Here we examine the spatiotemporal dynamics of CPC-dependent phosphorylation along microtubules throughout mitosis using a Förster resonance energy transfer-based sensor. We find that a CPC substrate phosphorylation gradient, with highest phosphorylation levels between the two spindle poles, emerges when a cell enters mitosis. Interestingly, this gradient becomes undetectable at metaphase, but can be revealed by partially suppressing CPC activity, suggesting that high substrate phosphorylation levels can mask persistent CPC-dependent spatial patterning. After anaphase onset, the gradient emerges and persists until cell cleavage. Selective mislocalization of the CPC during anaphase suppresses gradient formation, but overall substrate phosphorylation levels remain unchanged. Under these conditions, the spindle midzone fails to organize and function properly. Our findings suggest a model in which the CPC establishes phosphorylation gradients to coordinate the spatiotemporal dynamics needed for error-free cell division.

cytokinesis | cleavage furrow | Aurora B | Plk1 | RhoA

Dynamic microtubule-based structures are required for the stable propagation of genomes through cell division (1). It generally is agreed that these structures self-organize, a process by which complex architectures arise from the multiplicity of interactions involving key proteins that follow simple rules and respond to positional cues (2). These cues, which must vary on the relevant length-scale, can be mechanical (e.g., forces that unbind a protein from a microtubule or stall a motor protein) or chemical (e.g., a posttranslational modification that can activate an enzyme). At least two different chemical cues that form spatial gradients within single dividing cells have been described. First, a gradient of GTP-bound Ran can be observed before anaphase and contributes to metaphase spindle assembly (3, 4). Second, a gradient of phosphorylated substrates of the chromosomal passenger complex (CPC, comprised of Aurora B kinase, INCENP, Survivin, and Borealin) can be observed between segregating chromosomes during anaphase (5, 6). In contrast to the Ran gradient, the CPC substrate phosphorylation gradient remains poorly characterized, and its contributions to cell division remain untested.

The CPC is a widely conserved regulator of several processes required for mitosis, including bipolar spindle assembly, chromosome-microtubule attachment, and spindle midzone formation (5). To carry out these different functions, CPC localization changes through mitosis, with the protein complex binding along chromosomes when cells enter mitosis, concentrating at the inner centromeres before anaphase, and relocating to the spindle midzone upon anaphase onset (7). A spatial gradient of CPC substrate phosphorylation at anaphase was observed using Förster resonance energy transfer (FRET)-based sensors and antibody-based analyses (6). Because the peak of the substrate phosphorylation gradient coincides with CPC localization during anaphase, it is tempting to speculate that kinase localization determines the shape of the gradient. Consistent with this hypothesis, disruption of the spindle midzone using microtubule poisons or knockdown of mitotic kinesin-like protein 2 (MKLP2), a kinesin required for proper CPC localization, prevents the proper establishment of the spatial phosphorylation gradient (6). However, because these perturbations can interfere with other signaling pathways, such as Polo-like kinase (Plk) signaling (8), a proper test of the role of CPC localization in determining the shape of this spatial phosphorylation gradient is lacking.

Two different observations have raised the possibility that CPC-dependent spatial gradients are present before anaphase. First, phosphorylation levels of CPC substrates at centromeres/kinetochores depend on their distance from the inner centromere, where the CPC is concentrated (9). Second, chromosomes can enrich and activate the CPC (10), and therefore the probability of substrate phosphorylation is higher near chromosomes than at cell edges that can be several microns away. However, a spatial CPC substrate phosphorylation gradient has not been observed before anaphase.

Because CPC localization is dynamic, and there is extensive cellular reorganization during cell division, observing these gradients is likely to require live reporters of phosphorylation dynamics. The FRET-based sensors previously used to analyze the gradient in live cells did not reveal spatial phosphorylation gradients at earlier stages of cell division (6), perhaps largely because these sensors were targeted to chromosomes, and therefore phosphorylation dynamics could be analyzed only at cellular sites where chromosomes were present (Fig. S1) (6). Moreover, FRET sensors freely diffusing in the cytoplasm did not reveal spatial patterns of substrate phosphorylation, most likely because of the degradation of the gradient by diffusion of the sensors (6). Therefore, without a proper understanding of how and when the spatial phosphorylation gradient is established, it is difficult to alter its shape and examine its function.

Here, we used a microtubule-targeted FRET sensor to analyze the temporal and spatial dynamics of CPC substrate phosphor-

Author contributions: L.T. and T.M.K. designed research; L.T. performed research; L.T. analyzed data; and L.T. and T.M.K. wrote the paper.

The authors declare no conflict of interest.

This article is a PNAS Direct Submission.

[1]To whom correspondence should be addressed. E-mail: kapoor@rockefeller.edu.

This article contains supporting information online at www.pnas.org/lookup/suppl/doi:10.1073/pnas.1106748108/-/DCSupplemental.

ylation in dividing human cells. We found that a spatial gradient of CPC substrate phosphorylation appears when cells enter mitosis, is not detectable by the sensor at metaphase, reappears during anaphase, and persists until cells cleave. Further, we show that the shape of the phosphorylation gradient is coupled to CPC localization but does not depend on Plk activity or furrow ingression. By selectively mislocalizing the CPC during anaphase, we were able to alter the shape of the substrate phosphorylation gradient while retaining overall levels of phosphorylation. Under these conditions, the spindle midzone fails to assemble and function properly.

Results

We characterized the temporal dynamics of CPC substrate phosphorylation during cell division using our recently reported microtubule-targeted FRET sensor (11), the phosphorylation of which results in a conformational change that reduces energy transfer from CFP to YFP (Fig.1*A*). Time-lapse imaging of the sensor revealed that before nuclear envelope breakdown (NEB) the average CFP:YFP ratio was low (0.62 ± 0.04; $n > 10$ cells) (Fig. 1*B*), similar to that during interphase, when the CPC is down-regulated (12), and to that observed for the phosphorylation site mutated sensor (Thr to Ala) (shown in Fig. S2*M*). Together, these data suggest that this ratio likely corresponds to an unphosphorylated state of the sensor. As mitosis progressed, the average CFP:YFP ratio increased and then remained largely constant (CFP:YFP ratio 0.96 ± 0.06; $n > 10$ cells) (Fig. 1*B*) until anaphase onset (Fig. 1*C*). At anaphase, the average CFP:YFP ratios indicated that the sensor dephosphorylated slowly, with levels reducing ~20% toward the end of cleavage-furrow ingression (Fig. 1 *C* and *I*).

The microtubule-targeted FRET sensor allowed an analysis of changes in the gradient's shape over time in a single dividing cell. Interestingly, the microtubule-targeted FRET sensor revealed a spatial gradient at the very early stages of mitosis. Just after NEB, CFP:YFP emission ratios were highest at the center of the emerging bipolar spindle and were reduced toward astral microtubules that extended from spindle poles to the cell cortex (slope 0.02 ± 0.01 μm^{-1}; $n = 4$ cells) (Fig. 1 *D–F* and Fig. S3 *A–D*). By ~9 min the spatial gradient could not be detected (Fig. 1 *D Lower* and *F Lower*). Because we had not seen this transient gradient emerge using chromosome-targeted sensors, we exam-

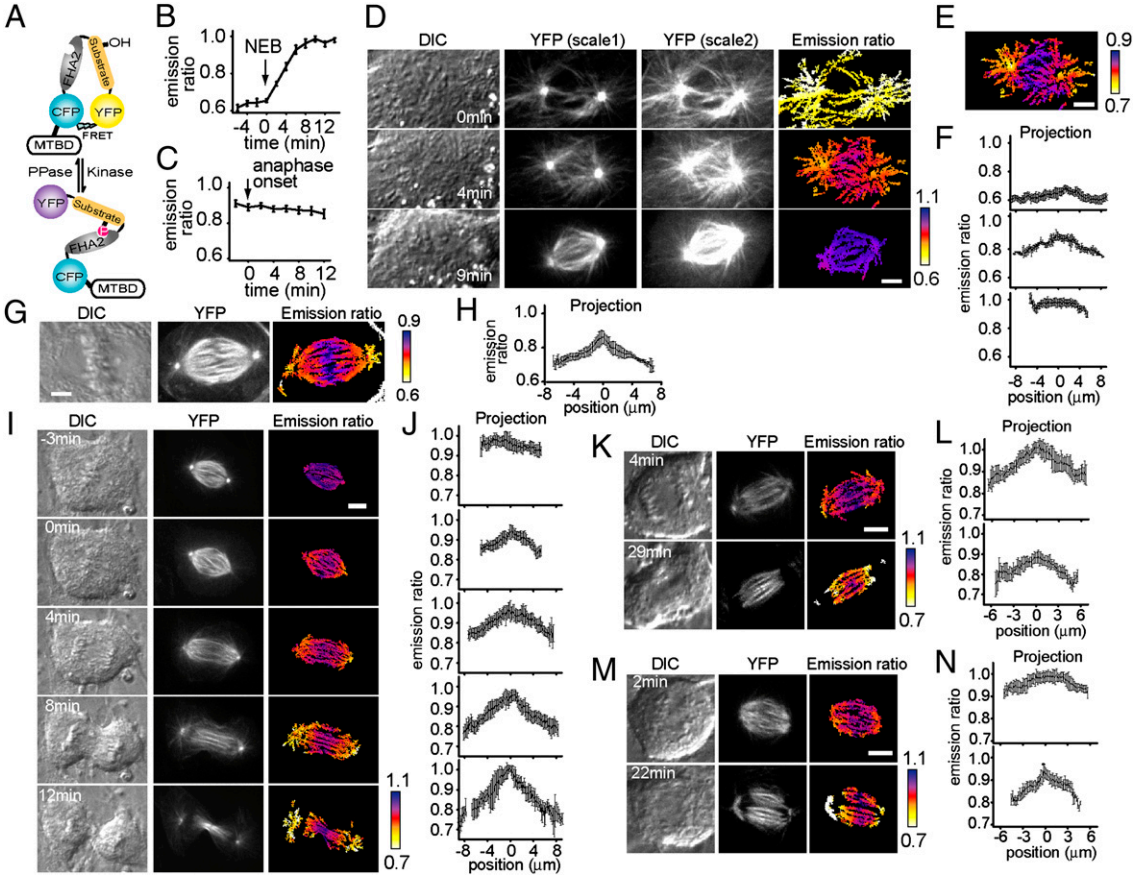

Fig. 1. A microtubule-targeted FRET sensor reveals a phosphorylation gradient for CPC substrates at different stages of cell division. (*A*) A schematic of the microtubule-targeted FRET sensor. Phosphorylation of the sensor leads to a conformational change that alters the CFP:YFP emission ratios. The microtubule-associated protein 4 microtubule-binding domain (MTBD) was used to target the sensor to microtubules. (*B*) The CFP:YFP emission ratio averaged for hTERT-RPE1 (human telomerase reverse transcriptase-immortalized retinal pigment epithelial cell line) cells expressing the microtubule-targeted sensor ($n > 10$) as they entered mitosis. Time 0 represents NEB. Error bars indicate SEM. (*C*) The same analysis was carried out for cells undergoing anaphase ($n > 10$). Time 0 represents anaphase onset. Error bars indicate SEM. (*D*) A cell expressing the microtubule-targeted FRET sensor was imaged through prophase–prometaphase. DIC, YFP (at two different contrast settings to reveal spindle as well as astral microtubules), and color-coded CFP:YFP emission ratio images are shown. Time 0 represents NEB. (*E*) Color-coded image of the CFP:YFP emission ratio from the 4-min time point in *D*, adjusted for a smaller range of emission ratios. (*F*) Averaged linescan projections along the spindle axis for the corresponding color-coded emission ratio images in *D*. Error bars indicate SD. (*G–N*) DIC, YFP, and color-coded emission ratio images, along with corresponding averaged linescan projections along the spindle axis, are shown for cells expressing the microtubule-targeted FRET sensor. A metaphase cell treated with 0.3 μM ZM447439 (*G* and *H*), a cell at anaphase (*I* and *J*), and cells at anaphase treated with 2 μM latrunculin B (*K* and *L*) or 250 nM BI2536 (*M* and *N*) are shown. Time 0 represents anaphase onset. Error bars indicate SD. (Scale bars, 5 μm.)

ined the response of the sensor after Aurora B RNAi knockdown or chemical inhibitor treatment. We found that, similar to the chromosome-targeted sensor, the majority of the microtubule-targeted sensor's response depended on the CPC at prometaphase, as it did at metaphase and anaphase (Fig. S2) (11). Although it is unlikely that the sensor can discriminate between closely related kinases (e.g., Aurora A and Aurora B), this response likely reflects functional differences between these kinases. Additional studies using antibodies to native phosphorylated substrates will be needed to analyze this Aurora B-dependent response further.

To examine whether the increasing levels of substrate phosphorylation (so that the "valleys" on either side of the peak are "filled") prevented detection of the CPC substrate phosphorylation gradient at metaphase, we used the Aurora kinase inhibitor ZM447439 to suppress overall phosphorylation partially. Because essentially complete inhibition of substrate phosphorylation is achieved at ~2 μM ZM447439 (13), we used 0.3 μM inhibitor for partial inhibition. Under these conditions, the average CFP:YFP ratio is 0.83 ± 0.04 (n = 47 cells), indicating that the substrate phosphorylation is suppressed partially and is comparable to that in anaphase cells (Fig. 1*C*). A spatial pattern similar to that observed at prometaphase, with CFP:YFP emission ratios peaking between the two spindle poles (the slope was comparable to that in prometaphase cells), was detected in a subset of cells (10/47) at metaphase (Fig. 1 *G* and *H*). In several other cells (11/47), an asymmetric pattern with maximal phosphorylation positioned away from the center of the spindle could be detected (Fig. S3 *E*–*H*). The reason for this asymmetry might be the presence of a single or a few chromosome(s) at one spindle pole, where the source of the gradient is positioned. These chromosomes are likely to be common when the CPC is inhibited (5) and are difficult to detect by differential interference contrast (DIC) imaging in rounded-up metaphase cells. We believe that the existence of misaligned chromosomes is likely to be the reason we cannot detect a robust gradient in approximately half of the metaphase cells imaged with low doses of the inhibitor. Together, these data are consistent with the hypothesis that increased levels of substrate phosphorylation at metaphase can mask CPC-dependent spatial patterning of phosphorylation. At this stage, we cannot exclude the possibility that these observations reflect limitations of our sensor-based analysis. Because we lack phospho-specific antibodies against endogenous CPC substrates that distribute uniformly across the spindle, additional tests remain difficult.

We next examined the spatial organization of CPC substrate phosphorylation during anaphase. Similar to results using chromatin-targeted sensors, the highest levels of phosphorylation coincided with the spindle midzone, and phosphorylation reduced toward each spindle pole (Fig. 1 *I* and *J*). In addition, the microtubule-targeted sensor revealed that the gradient emerged when chromosome segregation began. The slope of the gradient, as measured from its peak at the center of the spindle midzone toward a spindle pole, increased over time (from 0.02 ± 0.01 μm^{-1} before the appearance of the cleavage furrow to 0.04 ± 0.02 μm^{-1} after cleavage-furrow ingression starts; n = 16 cells) (Fig. 1*J*). Importantly, the site of maximum phosphorylation remained unchanged throughout anaphase (Fig. 1 *I* and *J*). Interestingly, the appearance of the anaphase gradient also coincided with decreasing phosphorylation after anaphase onset, consistent with our observation that decreased substrate phosphorylation at metaphase reveals CPC-dependent spatial patterning.

To analyze factors that contribute to the shape of the CPC substrate phosphorylation gradient, we focused on the analysis of cells undergoing anaphase. We first examined whether the CPC substrate phosphorylation gradient depended on successful cytokinesis. We blocked cleavage-furrow ingression by disrupting actin filament formation [using 2 μM latrunculin B (14)] or inhibiting Plk1 activity with a chemical inhibitor [BI2536 at 250 nM (15)]. Under either condition, the microtubule-targeted FRET sensor revealed that the shape of the CPC substrate phosphorylation gradient emerged and persisted for >20 min (Fig. 1 *K*–*N*), which was sufficient time for chromosome decondensation and cleavage-furrow ingression in unperturbed cells (Fig. 1*I*). These data show that the formation of the CPC substrate phosphorylation gradient at anaphase does not depend on cortical contraction or Plk1 signaling.

In principle, the gradient's shape is controlled by the intracellular localization of the kinase or the phosphatase, which serve as the phosphorylation "source" and "sink," respectively. The phosphatase(s) contributing to this phosphorylation gradient are not known. Therefore, we focused on altering the spatial distribution of CPC activity without inhibiting the kinase directly. The relocation of the CPC from centromeres to the spindle midzone depends on the dephosphorylation of INCENP at Thr-59 (16). Mutation of Thr-59 to glutamic acid affects CPC localization only after anaphase onset, without disrupting its metaphase functions (16). Therefore, we knocked down endogenous INCENP using RNAi and added back an mCherry-INCENP T59E mutant (hereafter referred to as "T59E-addback cells") or an mCherry-INCENP WT construct (hereafter referred to as "WT-addback cells") as a control (Fig. 2*A* and Fig. S4*A*). As anticipated, in T59E-addback cells, the CPC concentrated properly at centromeres before anaphase

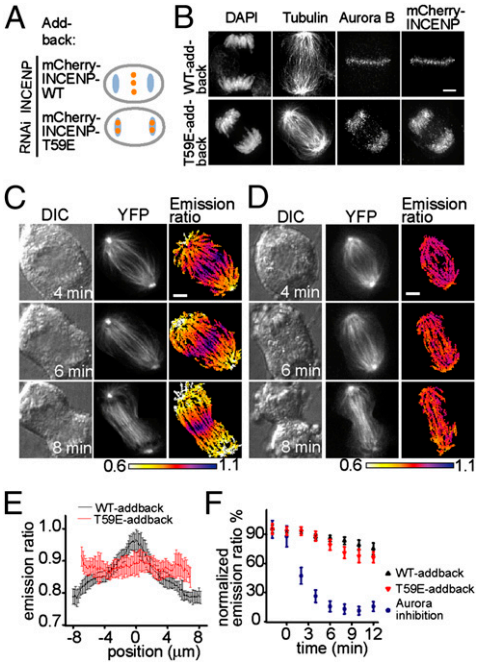

Fig. 2. The microtubule-targeted FRET sensor reveals that, although improper CPC localization disrupts the formation of the spatial phosphorylation gradient, average substrate phosphorylation remains unchanged. (*A*) A schematic of CPC (orange dot) mislocalization on chromosomes (blue) during anaphase. (*B*) WT-addback and T59E–addback cells were fixed and stained to label chromosomes (DAPI), tubulin, Aurora B, and mCherry-INCENP. (*C* and *D*) A WT-addback cell (*C*) or a T59E-addback cell (*D*) expressing the microtubule-targeted FRET sensor was imaged through anaphase. DIC, YFP, and color-coded emission ratio images are shown; timestamps are relative to anaphase onset. (*E*) Overlaid averaged linescan projections along the spindle axis for WT-addback and T59E-addback cells in *C* and *D*. Error bars indicate SD. (*F*) Cells expressing a microtubule-targeted sensor that are WT-addback cells (n > 10), T59E-addback cells (n > 20), or cells treated with Aurora kinase inhibitor ZM447439 (10 μM added at anaphase onset; n = 3) were imaged live through anaphase. The CFP:YFP emission ratio at each time point was averaged and normalized (setting the interphase ratio to 0 and the metaphase ratio to 100). Note that decreased emission ratio indicates dephosphorylation. Error bars indicate SEM. (Scale bars, 5 μm.)

(Fig. S4*B*) but remained enriched at chromosomal sites during anaphase and could not be detected at the spindle midzone (Fig. 2*B*).

We next examined CPC substrate phosphorylation in cells where the CPC was mislocalized. Although the microtubule-targeted sensor revealed a persistent gradient in WT-addback cells (Fig. 2 *C* and *E*), no robust spatial pattern of CPC substrate phosphorylation was apparent in T59E-addback cells throughout anaphase (Fig. 2 *D* and *E*). Importantly, the averaged CFP:YFP ratio was similar across microtubules in T59E- and WT-addback cells (Fig. 2 *E* and *F*). In contrast, when an Aurora kinase inhibitor was added to cells entering anaphase, the sensor revealed ~sevenfold lower average phosphorylation during cleavage-furrow ingression (t = 6 min onward) (Fig. 2*F*). Together, these data indicate that in T59E-addback cells the shape of the CPC substrate phosphorylation gradient was altered without significant changes in overall phosphorylation levels. Therefore, our data suggest that the shape of the substrate phosphorylation gradient is coupled to kinase localization.

We next asked whether kinase localization at the spindle midzone is sufficient for establishing a substrate phosphorylation gradient. Like the CPC, Plk1 localizes to the spindle midzone at anaphase (Fig. S5*A*) (8). We generated microtubule-targeted Plk sensors based on previously reported sensor of Plk activity (6, 17). The microtubule-targeted Plk sensor did not reveal spatial phosphorylation patterns, but Plk-dependent phosphorylation could be observed (Fig. S5 *B*–*H*). These data suggest that kinase localization alone is not likely to be sufficient to generate micrometer-scale gradients of substrate phosphorylation. At this stage, it is difficult to rule out the possibility that the lack of Plk-dependent spatial gradient is a limitation of the sensors we have used, and further experiments using phospho-specific antibodies against endogenous microtubule-bound Plk1 substrates are needed.

We next examined consequences of perturbing spatially organized CPC signaling. Because the CPC has numerous roles during anaphase, it is possible that the CPC localization at the midzone and the CPC substrate phosphorylation gradient may contribute to multiple processes such as spindle midzone formation (18, 19), compaction of anaphase chromosomes (20, 21), or the NoCut pathway (22, 23). We focused on spindle midzone formation and compared spindle midzone organization in T59E- vs. WT-addback cells using three different readouts. First, we examined the overall density and morphology of the midzone microtubules (Fig. 3 *A* and *C*). In contrast to cells in which the CPC was depleted or inhibited, which had dramatically altered anaphase spindle morphologies (18, 19) (Fig. S6), T59E-addback cells had spindle midzone microtubules that appeared similar to those of WT-addback cells. Second, we analyzed the localization of the CPC substrate mitotic kinesin-like protein 1 (MKLP1), a motor protein that binds the RhoA GTPase-activating protein, cytokinesis defect family member 4 (CYK-4) to form the centralspindlin complex (24). As expected, we found that MKLP1 was highly concentrated at the spindle midzone during anaphase in WT-addback cells (Fig. 3*A*). In contrast, in T59E-addback cells the level of MKLP1 at the spindle midzone was reduced significantly (threefold reduction indicated by linescans in Fig. 3 *A* and *B*). Third, we examined the extent of antiparallel microtubule overlap using protein regulator of cytokinesis 1 (PRC1), a nonmotor microtubule-associated protein that marks this cytoskeletal feature (25). In WT-addback cells, PRC1 localized to the spindle midzone (WT-addback cells in Fig. 3*C*). In contrast, in T59E-addback cells, PRC1 still associated with microtubules, but its localization extended over a wider region (twofold greater as indicated by linescans in Fig. 3 *C*–*E*). Together, these data show that the proper CPC localization and the spatial organization of its substrate phosphorylation are needed for spindle midzone assembly.

We next examined whether there are functional consequences of the spindle midzone disruption that we observed in cells

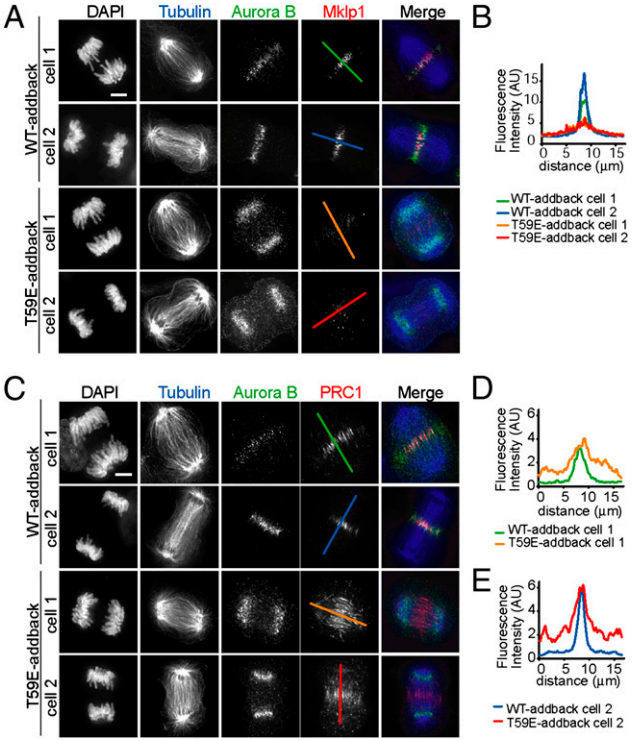

Fig. 3. Spatially organized CPC activity is needed for proper spindle midzone organization. (*A* and *C*) WT-addback and T59E-addback cells were fixed and stained to label chromosomes (DAPI), tubulin (blue), Aurora B (green), and MKLP1 (red in *A*) or PRC1 (red in *C*). (*B*, *D*, and *E*) Overlaid intensity linescans were generated using lines indicated in the images in *A* and *C*. (Scale bars, 5 μm.)

lacking spatially organized CPC signaling. Consistent with redundant signals from the spindle midzone and astral microtubules regulating cleavage-furrow formation (26), live-cell imaging of the T59E-addback cells revealed no overt defects in either positioning or ingression of the cleavage furrow (Fig. S7). Therefore, we needed to separate spindle midzone and astral microtubule signaling. To this end, we used a drug-synchronized monopolar cytokinesis assay (27). In this assay, astral microtubule distribution is symmetric initially, followed by the formation of a monopolar midzone at one end of the cell where a cleavage furrow ingresses (Fig. 4*A*). In T59E-addback cells, the CPC remained at chromosomal sites during anaphase (Fig. S8*A*), and a CPC substrate phosphorylation gradient could not be detected (Fig. 4 *B* and *C*), although overall substrate phosphorylation levels were maintained (Fig. 4*C*). Furthermore, consistent with the experiments analyzing bipolar cytokinesis, a properly organized midzone was not observed, and MKLP1 failed to localize to the microtubules (Fig. S8*B*). Moreover, the GTPase RhoA [a key regulator of contractile activity needed for cleavage-furrow ingression (26)], which localized at the site of cleavage in WT-addback cells undergoing monopolar cytokinesis (Fig. 4*D Upper*) (27), remained symmetrically distributed at the cell cortex in >90% of the T59E-addback cells (n > 50 cells) (Fig. 4 *D* and *E* and Fig. S8*C*). Importantly, cleavage-furrow ingression also was inhibited in these cells (Fig. S8 *C* and *D*). These data suggest that an organized spindle midzone is needed for proper RhoA localization and cleavage-furrow formation in monopolar cytokinesis.

We next analyzed if the cortical recruitment of RhoA also depends on a properly organized spindle midzone during bipolar cytokinesis. Because cleavage-furrow ingression was not blocked in T59E-addback cells, it was unlikely that RhoA failed to target. However, it was possible that the dynamics of RhoA recruitment

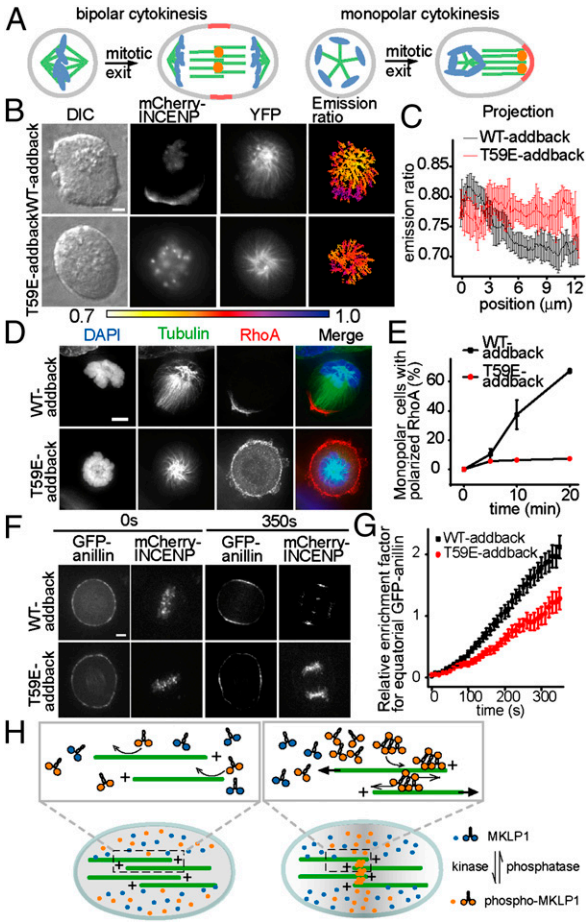

Fig. 4. Spatially organized CPC activity is needed for spindle midzone formation, RhoA clustering, cleavage during monopolar cytokinesis, and efficient anillin recruitment to the equatorial cortex during bipolar cytokinesis. (*A*) A schematic showing bipolar and monopolar cells undergoing mitotic exit. Chromosomes are shown in blue; microtubules in green; RhoA in red; and CPC as orange dots. (*B–E*) WT-addback and T59E-addback cells expressing the microtubule-targeted sensor were induced to undergo monopolar cytokinesis and analyzed as indicated. (*B* and *C*) DIC, mCherry-INCENP, YFP, and emission ratio images are shown in *B*. Overlaid linescan projections along the monopolar cell's long axis are shown in *C*. Error bars indicate SD. (*D* and *E*) Chromosomes (DAPI, blue), tubulin (green), and RhoA (red), and merged images are shown in *D*. Percentage of cells ($n \geq 600$) with polarized RhoA localization versus time after mitotic exit is triggered is shown in *E*. Error bars indicate SEM. (*F* and *G*) GFP-anillin and mCherry-INCENP images at anaphase onset (0 s) and 350 s after anaphase onset are shown in *F*. Relative enrichment of GFP-anillin at the equatorial cortex versus time for WT-addback cells ($n = 15$) and T59E-addback cells ($n = 12$) is shown in *G*. Error bars indicate SEM. (*H*) A schematic showing how the CPC may coordinate spindle midzone organization. Gray shading represents phosphorylation. (Scale bars, 5 μm.)

could be sensitive to the loss of the CPC substrate phosphorylation gradient. Quantitative analysis of the cortical signals for fluorophore-tagged human RhoA in live cells is limited by high cytosolic background (28). Therefore, we used GFP-tagged anillin, which is a scaffold protein linking RhoA to actomyosin at the cortex (29), as an alternative reporter for cleavage-furrow assembly. As expected, GFP-anillin distributed symmetrically in metaphase cells and concentrated to the site of cell cleavage within a few minutes after anaphase (Fig. 4*F Upper*). In contrast, GFP-anillin accumulated at the cortex in T59E-addback cells, but its levels were reduced (Fig. 4*F Lower*), and the recruitment kinetics were slower (~1.7 fold; $n > 10$ cells) (Fig. 4*G*). These data suggest that proper midzone organization is needed for the efficient assembly of the cleavage furrow in bipolar cytokinesis.

Discussion

Our findings show that the CPC establishes a substrate phosphorylation gradient early in mitosis with maximal phosphorylation centered between the two spindle poles. This gradient cannot be detected using FRET-based sensors during metaphase but appears again upon anaphase onset and persists through cell cleavage. These data suggest that the gradient is detected at stages of cell division when the overall CPC substrate phosphorylation is lower than that at metaphase, when substrate phosphorylation levels are highest, most likely because of the suppression of overall phosphatase activity (30) and robust CPC activation by chromosomes (10). Because partial suppression of substrate phosphorylation at metaphase can reveal a spatial gradient, we propose that increased levels of substrate phosphorylation can mask spatial gradients, although the CPC retains its capacity to generate such gradients.

It has been suggested that formation of intracellular signaling gradients involves the following three components. The first component is an effector molecule that exists in two states, S and S* (e.g., a motor protein in nonphosphorylated and phosphorylated forms). The second component is an enzyme (a source; e.g., a kinase) that converts S to S* and binds to a cellular structure (e.g., the spindle midzone). The third component is another enzyme (a sink; e.g., a phosphatase) that converts S* back to S and is localized in the cytoplasm or is bound to another cellular structure. S is converted to S* proximal to the location of the source. Diffusion moves S* away, allowing it to interact with the sink, which in turn regenerates S. The shape of the S* concentration gradient depends on the kinetics of interconversion between S and S* and on the diffusion coefficient of S*. This framework has been used to explain the Ran gradient (3) and can be used to describe our observations relating to the CPC substrate phosphorylation gradient. We find that the proper localization of CPC, which is the source, is important for establishing the spatial gradient at anaphase. At the spindle midzone, the CPC phosphorylates substrates, generating S*. These substrates diffuse away and then are acted on by phosphatases. Protein phosphatase 1-γ, a phosphatase that localizes to chromosomes during anaphase, and opposes CPC activity during metaphase (31), could be the relevant sink for phosphorylated CPC substrates at anaphase. When the CPC is mislocalized to chromosomes during anaphase, it could be insufficiently separated from the phosphatase, and thus no spatial gradient is observed. Further, consistent with the model, which indicates that rates of interconversion between S and S* are important for establishing a gradient, our findings suggest that the mechanisms of kinase activation and recruitment to substrates are critical. Plk localization is similar to that of the CPC at anaphase, but no spatial phosphorylation pattern is revealed using FRET sensors. An explanation for these differences could be that nonlinear increases in substrate phosphorylation at sites proximal to the kinase can be established by the CPC, whose activation depends on clustering and autophosphorylation (10), but not by Plk, which is targeted to its substrates via recognition of phospho-peptide docking sites (8). Finally, the diffusion of S*, a key parameter for establishing a gradient, needs to be limited through anchoring substrates to intracellular sites, because the gradient is not observed when FRET sensors diffuse freely in the cytoplasm. Proper tests of the contributions of these different factors likely will require in vitro reconstitution of the phosphorylation gradient with purified components.

Although CPC activity is needed for formation of the spindle midzone, our results show that defects in spindle midzone and cleavage-furrow assembly can be observed when total CPC substrate phosphorylation levels are unchanged but the spatial distribution of these posttranslational modifications is altered. Although different models can account for this observation, we

favor the model in which the proper localization of CPC at the spindle midzone sets up a gradient that allows threshold levels of phosphorylation to be achieved at specific intracellular sites. At anaphase onset, an initial shallow gradient becomes apparent, which may lead to highest levels of phosphorylated CPC substrates, such as MKLP1, at the center of the cell. It has been proposed that CPC phosphorylation relieves 14-3-3–mediated inhibition of MKLP1 and allows the motor to cluster into multiprotein assemblies that can make sufficiently long-lived associations with microtubules (32, 33). Therefore, local MKLP1 phosphorylation and clustering-dependent persistent filament binding and motility could lead to a rapid nonlinear increase in the levels of active MKLP1 at the center of a dividing cell (Fig. 4*H Right*). In contrast, uniform phosphorylation across the spindle microtubules could result in a distribution of phosphorylated MKLP1 so that the probability of interaction with another phosphorylated MKLP1 would be too low for clustering. As a result, MKLP1 would fail to slide microtubules to organize the spindle midzone properly (Fig. 4*H Left*). In normal cells, as the spindle midzone becomes more focused, possibly by MKLP1-dependent reductions in antiparallel filament overlap (34), the CPC becomes more concentrated in a narrower region, further sharpening the phosphorylation gradient, as we have observed.

It is likely that the contribution of the spatially organized CPC-dependent signaling to the regulation of different cell-division processes, such as chromosome condensation, spindle assembly, or the NoCut pathway, could vary and depend on the substrates' distinct phosphorylation kinetics, localization, and diffusion. For example, Oncoprotein 18 (Op18), a cytosolic substrate for CPC (10) and a microtubule destabilizer, is likely to function properly during anaphase without a CPC-dependent phosphorylation gradient (i.e., phosphorylation alone may be sufficient for its proper function, and spatially organized posttranslational modifications may not be needed). This hypothesis might explain our observation that the microtubule density in the anaphase spindle is not altered dramatically upon CPC mislocalization, whereas the midzone microtubule organization is affected. Interestingly, previous studies have suggested that a gradient of inactivated Op18 around mitotic chromosomes contributes to metaphase spindle assembly (35). It will be important to examine whether Op18 phosphorylation, which modulates Op18 binding to tubulin, also is organized spatially during anaphase and whether this organization is sensitive to CPC localization.

Our study suggests how a kinase may establish an intracellular spatial gradient of posttranslational marks to control cytoskeleton self-organization during the final stages of cell division. The robustness and precision with which this spatially organized CPC signaling determines the size and shape of the spindle midzone are not known. Further experimental studies analyzing chemical reaction rates, substrate diffusion, and timescales of protein activity, together with mathematical modeling, will be needed to determine whether the CPC-dependent phosphorylation gradient—like morphogen gradients critical for embryonic development—encodes positional information at limits set by basic physical principles (36).

Materials and Methods

Constructs used for FRET sensors were described previously (6, 11). mCherry-INCENP WT was constructed by cloning a human INCENP construct that is resistant to RNAi (a gift from S.M.A. Lens, Universitair Medisch Centrum Utrecht, The Netherlands) into the pMSCV N-terminal mCherry destination vector according to the Invitrogen gateway cloning manual. The mCherry-INCENP T59E mutant was generated by the quick-change method. GFP-anillin was constructed by cloning anillin cDNA (a gift from M. Glotzer, University of Chicago, Chicago, IL) into the pMSCV N-terminal GFP destination vector.

Other materials and methods are described in *SI Materials and Methods*.

ACKNOWLEDGMENTS. We thank M. Glotzer and S.M.A. Lens for reagents and M. A. Lampson for sharing unpublished data and reagents. T.M.K. received support from National Institutes of Health Grants GM65933 and GM65933-S1.

1. Walczak CE, Heald R, Kwang WJ (2008) Mechanisms of mitotic spindle assembly and function. *Int Rev Cytol* 265:111–158.
2. Nédélec F, Surrey T, Karsenti E (2003) Self-organisation and forces in the microtubule cytoskeleton. *Curr Opin Cell Biol* 15:118–124.
3. Bastiaens P, Caudron M, Niethammer P, Karsenti E (2006) Gradients in the self-organization of the mitotic spindle. *Trends Cell Biol* 16:125–134.
4. Kalab P, Heald R (2008) The RanGTP gradient—a GPS for the mitotic spindle. *J Cell Sci* 121:1577–1586.
5. Ruchaud S, Carmena M, Earnshaw WC (2007) Chromosomal passengers: Conducting cell division. *Nat Rev Mol Cell Biol* 8:798–812.
6. Fuller BG, et al. (2008) Midzone activation of aurora B in anaphase produces an intracellular phosphorylation gradient. *Nature* 453:1132–1136.
7. Carmena M, Earnshaw WC (2003) The cellular geography of aurora kinases. *Nat Rev Mol Cell Biol* 4:842–854.
8. Barr FA, Silljé HHW, Nigg EA (2004) Polo-like kinases and the orchestration of cell division. *Nat Rev Mol Cell Biol* 5:429–440.
9. Lampson MA, Cheeseman IM (2011) Sensing centromere tension: Aurora B and the regulation of kinetochore function. *Trends Cell Biol* 21:133–140.
10. Kelly AE, et al. (2007) Chromosomal enrichment and activation of the aurora B pathway are coupled to spatially regulate spindle assembly. *Dev Cell* 12:31–43.
11. Tseng BS, Tan L, Kapoor TM, Funabiki H (2010) Dual detection of chromosomes and microtubules by the chromosomal passenger complex drives spindle assembly. *Dev Cell* 18:903–912.
12. Honda R, Körner R, Nigg EA (2003) Exploring the functional interactions between Aurora B, INCENP, and survivin in mitosis. *Mol Biol Cell* 14:3325–3341.
13. Ditchfield C, et al. (2003) Aurora B couples chromosome alignment with anaphase by targeting BubR1, Mad2, and Cenp-E to kinetochores. *J Cell Biol* 161:267–280.
14. Foe VE, von Dassow G (2008) Stable and dynamic microtubules coordinately shape the myosin activation zone during cytokinetic furrow formation. *J Cell Biol* 183:457–470.
15. Petronczki M, Glotzer M, Kraut N, Peters J-M (2007) Polo-like kinase 1 triggers the initiation of cytokinesis in human cells by promoting recruitment of the RhoGEF Ect2 to the central spindle. *Dev Cell* 12:713–725.
16. Hümmer S, Mayer TU (2009) Cdk1 negatively regulates midzone localization of the mitotic kinesin Mklp2 and the chromosomal passenger complex. *Curr Biol* 19:607–612.
17. Macůrek L, et al. (2008) Polo-like kinase-1 is activated by Aurora A to promote checkpoint recovery. *Nature* 455:119–123.
18. Speliotes EK, Uren A, Vaux D, Horvitz HR (2000) The survivin-like *C. elegans* BIR-1 protein acts with the Aurora-like kinase AIR-2 to affect chromosomes and the spindle midzone. *Mol Cell* 6:211–223.
19. Hauf S, et al. (2003) The small molecule Hesperadin reveals a role for Aurora B in correcting kinetochore-microtubule attachment and in maintaining the spindle assembly checkpoint. *J Cell Biol* 161:281–294.
20. Mora-Bermúdez F, Gerlich D, Ellenberg J (2007) Maximal chromosome compaction occurs by axial shortening in anaphase and depends on Aurora kinase. *Nat Cell Biol* 9:822–831.
21. Neurohr G, et al. (2011) A midzone-based ruler adjusts chromosome compaction to anaphase spindle length. *Science* 332:465–468.
22. Norden C, et al. (2006) The NoCut pathway links completion of cytokinesis to spindle midzone function to prevent chromosome breakage. *Cell* 125:85–98.
23. Steigemann P, et al. (2009) Aurora B-mediated abscission checkpoint protects against tetraploidization. *Cell* 136:473–484.
24. Mishima M, Kaitna S, Glotzer M (2002) Central spindle assembly and cytokinesis require a kinesin-like protein/RhoGAP complex with microtubule bundling activity. *Dev Cell* 2:41–54.
25. Subramanian R, et al. (2010) Insights into antiparallel microtubule crosslinking by PRC1, a conserved nonmotor microtubule binding protein. *Cell* 142:433–443.
26. Eggert US, Mitchison TJ, Field CM (2006) Animal cytokinesis: From parts list to mechanisms. *Annu Rev Biochem* 75:543–566.
27. Hu C-K, Coughlin M, Field CM, Mitchison TJ (2008) Cell polarization during monopolar cytokinesis. *J Cell Biol* 181:195–202.
28. Roberts PJ, et al. (2008) Rho Family GTPase modification and dependence on CAAX motif-signaled posttranslational modification. *J Biol Chem* 283:25150–25163.
29. Piekny AJ, Glotzer M (2008) Anillin is a scaffold protein that links RhoA, actin, and myosin during cytokinesis. *Curr Biol* 18:30–36.
30. Mochida S, Hunt T (2007) Calcineurin is required to release Xenopus egg extracts from meiotic M phase. *Nature* 449:336–340.
31. Liu D, et al. (2010) Regulated targeting of protein phosphatase 1 to the outer kinetochore by KNL1 opposes Aurora B kinase. *J Cell Biol* 188:809–820.
32. Hutterer A, Glotzer M, Mishima M (2009) Clustering of centralspindlin is essential for its accumulation to the central spindle and the midbody. *Curr Biol* 19:2043–2049.
33. Douglas ME, Davies T, Joseph N, Mishima M (2010) Aurora B and 14-3-3 coordinately regulate clustering of centralspindlin during cytokinesis. *Curr Biol* 20:927–933.
34. Nislow C, Lombillo VA, Kuriyama R, McIntosh JR (1992) A plus-end-directed motor enzyme that moves antiparallel microtubules in vitro localizes to the interzone of mitotic spindles. *Nature* 359:543–547.
35. Niethammer P, Bastiaens P, Karsenti E (2004) Stathmin-tubulin interaction gradients in motile and mitotic cells. *Science* 303:1862–1866.
36. Gregor T, Tank DW, Wieschaus EF, Bialek W (2007) Probing the limits to positional information. *Cell* 130:153–164.